

RESIDE: A Benchmark for Single Image Dehazing

Boyi Li*, Wenqi Ren*, Member, IEEE, Dengpan Fu, Dacheng Tao, Fellow, IEEE, Dan Feng, Member, IEEE, Wenjun Zeng, Fellow, IEEE and Zhangyang Wang, Member, IEEE.

Abstract—In this paper, we present a comprehensive study and evaluation of existing single image dehazing algorithms, using a new large-scale benchmark consisting of both synthetic and real-world hazy images, called REalistic Single Image DEhazing (RESIDE). RESIDE highlights diverse data sources and image contents, and is divided into five subsets, each serving different training or evaluation purposes. We further provide a rich variety of criteria for dehazing algorithm evaluation, ranging from full-reference metrics, to no-reference metrics, to subjective evaluation and the novel task-driven evaluation. Experiments on RESIDE sheds light on the comparisons and limitations of state-of-the-art dehazing algorithms, and suggest promising future directions.

Index Terms—Dehazing, Detection, Dataset, Evaluations.

I. INTRODUCTION

A. Problem Description: Single Image Dehazing

Images captured in outdoor scenes often suffer from poor visibility, reduced contrasts, fainted surfaces and color shift, due to the presence of haze. Caused by aerosols such as dust, mist, and fumes, the existence of haze adds complicated, nonlinear and data-dependent noise to the images, making the haze removal (a.k.a. *dehazing*) a highly challenging image restoration and enhancement problem. Moreover, many computer vision algorithms can only work well with the scene radiance that is haze-free. However, a dependable vision system must reckon with the entire spectrum of degradations from unconstrained environments. Taking autonomous driving for example, hazy and foggy weather will obscure the vision of on-board cameras and create confusing reflections and glare, leaving state-of-the-art self-driving cars in struggle [1]. Dehazing is thus becoming an increasingly desirable technique for both computational photography and computer vision tasks, whose advance will immediately benefit many blooming application fields, such as video surveillance and autonomous/assisted driving.

Boyi Li and Dan Feng are with the Wuhan National Laboratory for Optoelectronics, Huazhong University of Science and Technology, Wuhan, China. Email: boyilics@gmail.com, dfeng@hust.edu.cn.

Wenqi Ren is with State Key Laboratory of Information Security, Institute of Information Engineering, Chinese Academy of Sciences. Email: rwq.renwenqi@gmail.com.

Dengpan Fu is with Department of Electronic Engineering and Information Science, University of Science and Technology of China. Email: fdpan@mail.ustc.edu.cn.

Dacheng Tao is with the Centre for Quantum Computation and Intelligent Systems and the Department of Engineering and Information Technology, University of Technology Sydney, Sydney, NSW 2007, Australia. Email: dacheng.tao@sydney.edu.au.

Wenjun Zeng is with Microsoft Research, Beijing, China. Email: wezeng@microsoft.com.

Zhangyang Wang is with the Department of Computer Science and Engineering, Texas A&M University, USA, and is the corresponding author. Email: atlaswang@tamu.edu

The first two authors contribute equally.

While some earlier works consider multiple images from the same scene to be available for dehazing [2], [3], [4], [5], the *single image dehazing* proves to be a more realistic setting in practice, and thus gained the dominant popularity. The *atmospheric scattering model* has been the classical description for the hazy image generation [6], [7], [8]:

$$I(x) = J(x)t(x) + A(1 - t(x)), \quad (1)$$

where $I(x)$ is observed hazy image, $J(x)$ is the haze-free scene radiance to be recovered. There are two critical parameters: A denotes the global atmospheric light, and $t(x)$ is the transmission matrix defined as:

$$t(x) = e^{-\beta d(x)}, \quad (2)$$

where β is the scattering coefficient of the atmosphere, and $d(x)$ is the distance between the object and the camera.

We can re-write the model (1) for the clean image as the output:

$$J(x) = \frac{1}{t(x)}I(x) - A\frac{1}{t(x)} + A. \quad (3)$$

Most state-of-the-art single image dehazing methods exploit the physical model (1), and estimate the key parameters A and $t(x)$ in either physically grounded or data-driven ways. The performance of the top methods have continuously improved [9], [10], [11], [12], [13], [14], especially after the latest models embracing deep learning [15], [16], [17].

B. Existing Methodology: An Overview

Given the atmospheric scattering model, most dehazing methods follow a similar three-step methodology: (1) estimating the transmission matrix $t(x)$ from the hazy image $I(x)$; (2) estimating A using some other (often empirical) methods; (3) estimating the clean image $J(x)$ via computing (3).

Usually, the majority of attention is paid to the first step, which can rely on either physically grounded priors or fully data-driven approaches.

A noteworthy portion of dehazing methods exploited natural image priors and depth statistics. [18] imposed locally constant constraints of albedo values together with decorrelation of the transmission in local areas, and then estimated the depth value using the albedo estimates and the original image. It did not constrain the scenes depth structure, thus often leads to the inaccurate estimation of color or depth. [19], [20] discovered the dark channel prior (DCP) to more reliably calculate the transmission matrix, followed by many successors. However, the prior is found to be unreliable when the scene objects are similar to the atmospheric light [16]. [11] enforced the boundary constraint and contextual regularization for sharper restorations. [13] developed a color attenuation prior and

created a linear model of scene depth for the hazy image, and then learned the model parameters in a supervised way. [21] jointly estimated scene depth and recover the clear latent image from a foggy video sequence. [14] proposed a non-local prior, based on the assumption that each color cluster in the clear image became a haze-line in RGB space.

In view of the prevailing success of Convolutional Neural Networks (CNNs) in computer vision tasks, several dehazing algorithms have relied on various CNNs to directly learn $t(x)$ fully from data, in order to avoid the often inaccurate estimation of physical parameters from a single image. DehazeNet [15] proposed a trainable model to estimate the transmission matrix from a hazy image. [16] came up with a multi-scale CNN (MSCNN), that first generated a coarse-scale transmission matrix and gradually refined it. Despite their promising results, *the inherent limitation of training data is becoming a increasingly severe obstacle for this booming trend*: see Section 2.1 for more discussions.

Besides, a few efforts have been made beyond the sub-optimal procedure of separately estimating parameters, which will cause accumulated or even amplified errors, when combining them together to calculate (3). They instead advocate simultaneous and unified parameter estimation. Earlier works [22], [23] modeled the hazy image with a factorial Markov random field, where $t(x)$ and A were two statistically independent latent layers. Another line of researches [24], [25] try to make use of Retinex theory to approximate the spectral properties of object surfaces by the ratio of the reflected light. Very recently, [17] presented a re-formulation of (2) to integrate $t(x)$ and A into one new variable. As a result, their CNN dehazing model was fully end-to-end: $J(x)$ was directly generated from $I(x)$, without any intermediate parameter estimation step. The idea was later extended to video dehazing in [26].

C. Our Contribution

Despite the prosperity of single image dehazing algorithms, there have been two key hurdles to the further development of this field: (1) there has been no large-scale, realistic benchmark dataset so far for image dehazing; (2) current metrics for evaluating and comparing image dehazing algorithms are neither convincing nor sufficient. Detailed discussions will be presented in Section 2.

This paper is directly motivated to overcome the above two hurdles, and makes three-fold technical contributions:

- We introduce the first-of-its-kind benchmark, called the *Realistic Single Image Dehazing (RESIDE)* dataset. An overview of RESIDE could be found in Tables I, II, and image examples are displayed in Figure 1. Compared with exiting synthetic training and testing sets of unrealistic indoor scenes, the RESIDE dataset includes a large diversity of both indoor and outdoor scene images for training, as well as real-world hazy images in addition to synthetic ones for evaluation. Specially, we annotate a set of 4,322 real-world hazy images with object bounding boxes.
- We bring in an innovative set of evaluation strategies in accordance with the new RESIDE dataset. Besides

TABLE I
OVERVIEW OF RESIDE: DATA SOURCES AND CONTENTS

Type	Number
Synthetic Indoor Hazy Images	110,500
Synthetic Outdoor Hazy Images	313,950
Realistic Hazy Images (Unannotated)	4,807
Realistic Annotated Hazy Images	4,322

the widely adopted PSNR and SSIM, we further employ both no-reference metrics and human subjective scores to evaluate the dehazing results, especially for real-world hazy images without clean groundtruth. More importantly, we recognize that image dehazing in practice usually serves as the preprocessing step for mid-level and high-level vision tasks. We thus propose to exploit the object detection performance on the dehazed images as a brand-new “task-specific” evaluation criterion for dehazing algorithms.

- We conduct an extensive and systematic range of experiments to quantitatively compare nine state-of-the-art single image dehazing algorithms, using the new RESIDE dataset and the proposed variety of evaluation criteria. Our evaluation and analysis demonstrate the performance and limitations of state-of-the-art algorithms. The findings from these experiments not only confirm what is commonly believed, but also suggest new research directions in single image dehazing.

The RESIDE dataset will be made publicly available soon for research purposes on our project’s website¹. The manuscript will be periodically updated to include more benchmarking results.

II. DATASET AND EVALUATION: STATUS QUO

A. Training Data

Many image restoration and enhancement tasks benefit from the continuous efforts for standardized benchmarks to allow for comparison of different proposed methods under the same conditions, such as [27], [28]. In comparison, a common large-scale benchmark has been long missing for dehazing, owing to the significant challenge in collecting or creating realistic hazy images with clean groundtruth references. It is generally impossible to capture the same visual scene with and without haze, while all other environment conditions stay identical. Therefore, recent dehazing models [29], [30] typically generate their training sets by creating synthetic hazy images from clean ones: they first obtain depth maps of the clean images, by either utilizing available depth maps for depth image datasets, or estimating the depth [31]; and then generate the hazy images by computing (1). Data-driven dehazing models could then be trained to regress clean images from hazy ones.

Fattal’s dataset [29] provided 12 synthetic images. FRIDA [32] produced a set of 420 synthetic images, for evaluating the performance of automatic driving systems in various hazy environments. Both of them are too small to train effective

¹<https://sites.google.com/site/boyilics/website-builder/reside>

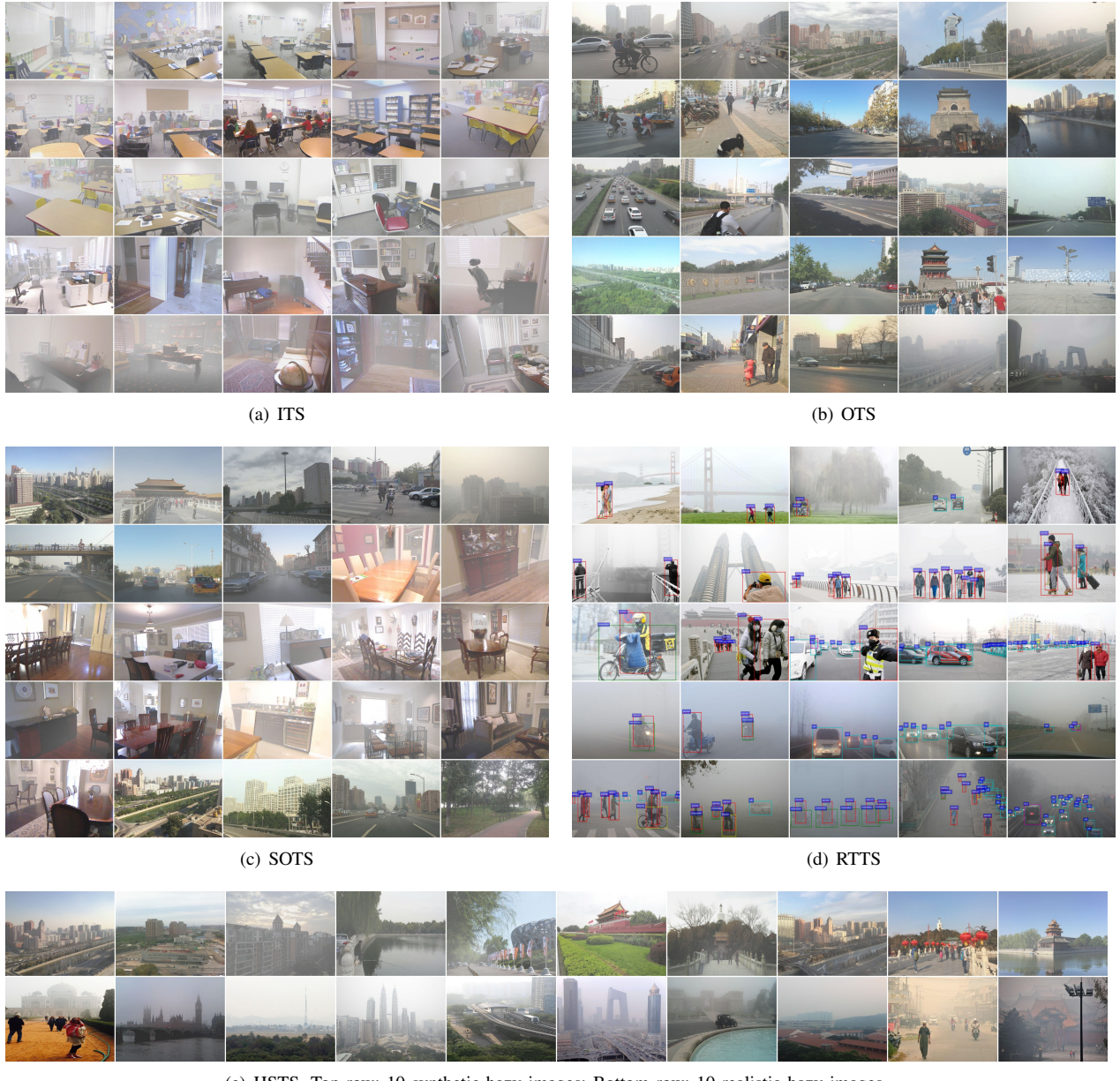


Fig. 1. Example images from the five sets in RESIDE (see Table II)

TABLE II
STRUCTURE OF RESIDE: FIVE SUBSETS FOR TRAINING AND TESTING

Subset	Number
Indoor Training Set (ITS)	110,000
Outdoor Training Set (OTS)	313,950
Synthetic Objective Testing Set (SOTS)	1,000
Real-world Task-driven Testing Set (RTTS)	4,322
Hybrid Subjective Testing Set (HSTS)	20

dehazing models. To form large-scale training sets, [16], [17] used the ground-truth images with depth meta-data from the indoor NYU2 Depth Database [33] and the Middlebury stereo database [34]. Recently, [30] generated Foggy Cityscapes dataset with 20,550 images from the Cityscapes dataset, using

incomplete depth information.

Despite their positive driving effects in the development of dehazing algorithms, those synthetic images for training have inevitably brought in two limitations. On the one hand, many depth image datasets used to generate synthetic images, e.g., [33], [34], are collected from indoor scenes, while dehazing is applied to outdoor environments. The content of training data thus significantly diverges from the target subjects in real dehazing applications. Such a mismatch will undermine the practical effectiveness of the trained dehazing models. On the other hand, while a limited number of outdoor datasets [35], [30] have been utilized, their depth information is either incomplete or inaccurate, often leading to unrealistic hazy images and artifacts during synthesis.

B. Testing Data and Evaluation Criteria

The testing sets in use are mostly synthetic hazy images with known groundtruth too, although some algorithms were also visually evaluated on real hazy images [16], [15], [17].

With multiple dehazing algorithms available, it becomes pivotal to find appropriate evaluation criteria to compare their dehazing results. Most dehazing algorithms rely on the full-reference PSNR and SSIM metrics, with assuming a synthetic testing set with known clean groundtruth too. As discussed above, their practical applicability may be in jeopardy even a promising testing performance is achieved, due to the large content divergence between synthetic and real hazy images. To objectively evaluate dehazing algorithms on real hazy images without reference, no-reference image quality assessment (IQA) models [36], [37], [38] are possible candidates. [39] tested a few no-reference objective IQA models among several dehazing approaches on their self-collected set of 25 hazy images, but did not compare any latest CNN-based dehazing models.

PSNR/SSIM, as well as other objective metrics, often align poorly with human perceived visual qualities [39]. Many papers visually display dehazing results, but the result differences between state-of-the-art dehazing algorithms are often too subtle for people to reliably judge. That suggests the necessity of conducting a subjective user study, towards which few efforts have been made so far [40], [39].

It has been recognized that the performance of high-level computer vision tasks, such as object detection and recognition, will deteriorate in the presence of various degradations, and is thus largely affected by the quality of image restoration and enhancement. Dehazing could be used as pre-processing for many computer vision tasks executed in the wild, and the resulting task performance could in turn be treated as an indirect indicator of the dehazing quality. Such a “task-driven” evaluation way has received little attention so far, despite its great implications for outdoor applications. A relevant preliminary effort was presented in [17], where the authors compared a few CNN-based dehazing models by placing them in an object detection pipeline, but their tests were on synthetic hazy data with bounding boxes. [30] created a dataset of 101 real-world images depicting foggy driving scenes, which came with ground truth annotations for evaluating semantic segmentation and object detection. Besides being relatively small, their dataset cannot be used for evaluating dehazing perceptual quality, either objectively or subjectively .

III. A NEW DATASET: RESIDE

We propose the *REalistic Single Image DEhazing* (**RESIDE**) dataset, a new large-scale dataset for benchmarking single image dehazing algorithms. RESIDE is built to be comprehensive and diverse in data sources (synthetic versus real world), contents (indoor versus outdoor scenes), and evaluation options (see Section 4 for details).

A. RESIDE Training Set

The REISDE training set consists of *Indoor Training Set* (ITS) and *Outdoor Training Set* (OTS), both of which are

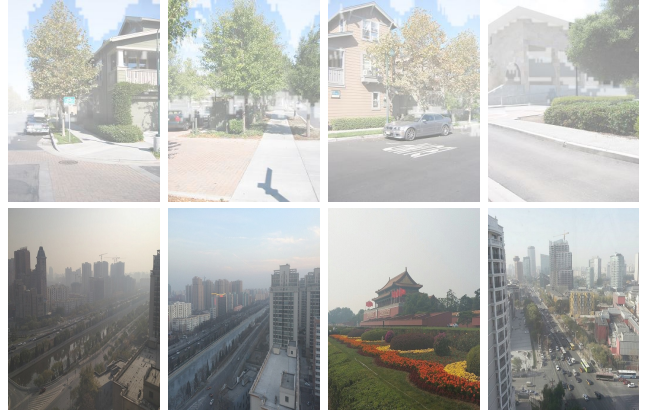


Fig. 2. Visual comparison between the synthetic hazy images directly generated from Make3D and from OTS. The first and second rows are the synthesized hazy images based on the Make3D dataset and our OTS, respectively.

synthetic images but from distinct sources and synthesis ways. ITS contains 110,000 synthetic hazy images, generated using images from existing indoor depth datasets such as NYU2 [33] and Middlebury stereo [34]. An optional split of 100,000 for training and 10,000 for validation is provided. OTS contains 313,950 images synthesized from collected real world outdoor scenes [41], without depth information. We use [31] to estimate the depth map for each image, with which we synthesize outdoor hazy images.

For generating both synthetic sets, We set different atmospheric lights A , by choosing each channel uniformly between $[0.6, 1.0]$, and select $\beta \in \{0.4, 0.6, 0.8, 1.0, 1.2, 1.4, 1.6\}$. Both ITS and OTS thus contains paired clean and hazy images, where a clean groundtruth image can leads to multiple pairs whose hazy images are generated under different parameters A and β .

One straightforward option would be to utilize a few existing depth datasets collected from outdoor scene such as Make3D [35] and KITTI [42]. However, the outdoor depth maps tend to be very unreliable. Due to the limitations of RGB-based depth cameras, the Make3D dataset suffer from at least 4 meters of average root mean squared error in the predicted depths, and the KITTI dataset has at least 7 meters of average error [43]. In comparison, the average depth errors in indoor datasets, e.g., NYU-Depth-v2 [33], are usually as small as 0.5 meter. For the outdoor depth maps can also contain a large amount of artifacts and large holes, which renders it inappropriate for direct use in haze simulation. In comparison, [31] is observed to produce more accurate depth maps and lead to artifact-free hazy images. Visual comparisons between the synthetic hazy images directly generated from Make3D [35] and from OTS are included in Figure 2. Another possible alternative is to adopt recent approaches of depth map denoising and in-painting [44], which we leave for future exploration.

B. RESIDE Testing Set

The REISDE testing set is composed of three components: *Synthetic Objective Testing Set* (SOTS), *Real-world Task-*

TABLE III
DETAILED CLASSES INFORMATION OF RTTS.

Category	<i>person</i>	<i>bicycle</i>	<i>car</i>	<i>bus</i>	<i>motorbike</i>	Total
Normal	7,950	534	18,413	1,838	862	29,597
Difficult	3,416	164	6,904	752	370	11,606
Total	11,366	698	25,317	2,590	1,232	41,203

driven Testing Set (RTTS), and the *Hybrid Subjective Testing Set* (HSTS), each corresponding to a different evaluation viewpoint. SOTS selects 500 indoor images from NYU2 [33] and 500 outdoor scenes from internet (non-overlapping with images in ITS and OTS), and follow the same process as ITS to synthesize hazy images. We specially create challenging dehazing cases for testing, e.g., white scenes added with heavy haze. HSTS picks 10 synthetic outdoor hazy images generated in the same way as OTS, together with 10 real-world hazy images, combined for human subjective review.

RTTS collects 4,322 real-world hazy images crawled from the web, covering mostly traffic and driving scenarios. Each image is annotated with object categories and bounding boxes, and RTTS is organized in the same form as VOC2007 [45]. We currently focus on five traffic-related categories: car, bicycle, motorbike, person, bus. We obtain 41,203 annotated bounding boxes, 11,606 of which are marked as “difficult” and not used in this paper’s experiments. The class details of RTTS are show in III. Additionally, we also collect 4,807 unannotated real-world hazy images, which are not exploited in this paper, but may potentially be used for domain adaption in future, etc.

IV. A NEW MINDSET FOR DEHAZING EVALUATION

A. From Full-Reference to No-Reference

Despite the popularity of the full-reference PSNR/SSIM metrics for evaluating dehazing algorithms, they are inherently limited due to the unavailability of clean groundtruth images in practice, as well as their often poor alignment with human perception quality [39]. We thus refer to two no-reference IQA models: spatsialspectral entropy-based quality (SSEQ) [38], and blind image integrity notator using DCT statistics (BLIINDS-II) [37], to complement the shortness of PSNR/SSIM. Note that the score of SSEQ and BLIINDS2 used in [38] and [37] are range from 0 (best) to 100 (worst), and we reverse the score to make the correlation consistent to full-reference metrics.

We will apply PSNR, SSIM, SSEQ, and BLIINDS-II, to the dehazed results on SOTS, and examine how consistent their resulting ranking of dehazing algorithms will be. We will also apply the four metrics on HSTS (PSNR and SSIM are only computed on the 10 synthetic images), and further compare those objective measures with subjective ratings.

B. From Objective to Subjective

[39] investigated various choices of full-reference and no-reference IQA models, and found them to be limited in predicting the quality of dehazed images. We then conduct a subjective user study on the quality of dehazing results produced by different algorithms, from which we gain more

useful observations. Groundtruth images are also included when they are available as references.

In the previous survey [39] a participant scored each dehazing result image with an integer from 1 to 10 that best reflects its perceptual quality. We make two important innovations: (1) asking participants to give pairwise comparisons rather than individual ratings, the former often believed to be more robust and consistent in subjective surveys; (2) decomposing the perceptual quality into two dimensions: the dehazing *Clearness* and *Authenticity*, the former defined as how thoroughly the haze has been removed, and the latter defined as how realistic the dehazed image looks like. Such two disentangled dimensions are motivated by our observations that some algorithms produce naturally-looking results but are unable to fully remove haze, while some others remove the haze at the price of unrealistic visual artifacts.

During the survey, each participant is shown a set of dehazed result pairs obtained using two different algorithms for the same hazy image. For each pair, the participant needs to decide which one is better than the other in terms of clearness, and then which one is better for Authenticity. The image pairs are drawn from all the competitive methods randomly, and the images winning the pairwise comparison will be compared again in the next round, until the best one is selected. We fit a Bradley-Terry [46] model to estimate the subjective scores for each dehazing algorithm so that they can be ranked. More details on the subjective survey are included in the supplementary.

C. From Signal-Level to Task-Driven

Since dehazed images are often subsequently fed for automatic semantic analysis tasks such as recognition and detection, we argue that the optimization target of dehazing in these tasks is neither pixel-level or perceptual-level quality, but the utility of the dehazed images in the given semantic analysis task [47]. We thus propose the task-driven evaluation for dehazing algorithms, and study the problem of object detection in the presence of haze as an example. We notice that [30] investigated detection and segmentation problems in hazy images as well, but not for the dehazing evaluation purpose. Specially, we used the same pre-trained Faster R-CNN [48] model to detect the objects of interests, from the dehazed results of RTTS by various algorithms, and rank all algorithms via the mean Average Precision (mAP) achieved.

V. EXPERIMENTAL COMPARISON

Based on the rich resources provided by RESIDE, we evaluate 9 representative state-of-the-art algorithms: Dark-Channel Prior (DCP) [9], Fast Visibility Restoration (FVR) [10], Boundary Constrained Context Regularization (BCCR) [11], Artifact Suppression via Gradient Residual Minimization (GRM) [12], Color Attenuation Prior (CAP) [13], Non-local Image Dehazing (NLD) [14], DehazeNet [15], Multi-scale CNN (MSCNN) [16], and All-in-One Dehazing Network (AOD-Net) [17]. The last three belong to the latest CNN-based dehazing algorithms. For all data-driven algorithms, they are trained on the entire RESIDE training set: ITS + OTS.

TABLE IV
AVERAGE FULL- AND NO-REFERENCE EVALUATIONS RESULTS OF DEHAZED RESULTS ON SOTS.

	DCP [9]	FVR [10]	BCCR [11]	GRM [12]	CAP [13]	NLD [14]	DehazeNet [15]	MSCNN [16]	AOD-Net [17]
500 synthetic indoor images in SOTS									
PSNR	18.87	18.02	17.87	20.44	21.31	18.53	22.66	20.01	21.01
SSIM	0.7935	0.7256	0.7701	0.8233	0.8247	0.7018	0.8325	0.7907	0.8372
SSEQ	64.94	67.75	65.83	63.30	64.69	67.46	65.46	65.22	67.65
BLIINDS-II	74.41	76.13	65.45	66.67	73.41	74.85	71.71	74.49	78.94
500 synthetic outdoor images in SOTS									
PSNR	18.54	16.61	17.71	20.77	23.95	19.52	26.84	21.73	24.08
SSIM	0.7100	0.7236	0.7409	0.7617	0.8692	0.7328	0.8264	0.8313	0.8726
SSEQ	83.59	82.87	83.04	76.18	81.74	84.10	81.65	81.46	84.13
BLIINDS-II	89.12	86.72	89.43	82.98	85.93	86.32	83.60	86.72	87.43

TABLE V
AVERAGE SUBJECTIVE SCORES, AS WELL AS FULL- AND NO-REFERENCE EVALUATIONS RESULTS, OF DEHAZING RESULTS ON HSTS.

	DCP [9]	FVR [10]	BCCR [11]	GRM [12]	CAP [13]	NLD [14]	DehazeNet [15]	MSCNN [16]	AOD-Net [17]
Synthetic images									
Clearness	1.26	0.18	0.62	0.75	0.50	1	0.29	1.22	0.86
Authenticity	0.78	0.14	0.50	0.95	0.86	1	1.94	0.54	1.41
PSNR	17.27	15.68	16.61	20.48	22.88	18.92	26.94	20.53	23.41
SSIM	0.7210	0.7157	0.6947	0.7631	0.8223	0.7411	0.8758	0.7893	0.8616
SSEQ	86.15	85.68	85.60	78.43	85.32	86.28	86.01	85.56	86.75
BLIINDS-II	90.70	87.65	91.05	82.30	85.75	85.30	87.15	88.70	87.50
Real-world images									
Clearness	0.39	0.46	0.45	0.75	1	0.54	1.16	1.29	1.05
Authenticity	0.17	0.20	0.18	0.62	1	0.15	1.03	1.27	1.07
SSEQ	68.65	67.75	66.63	70.19	67.67	67.96	68.34	68.44	70.05
BLIINDS-II	69.35	72.10	68.55	79.60	63.55	70.80	60.35	62.65	74.75

A. Objective Comparison on SOTS

We first compare the dehazed results on SOTS using two full-reference (PSNR, SSIM) and two no-reference metrics (SSEQ, BLIINDS-II). Table IV displays the detailed scores of each algorithm in terms of each metric.²

In general, since learning-based methods [15], [13], [16], [17] are optimized by directly minimizing the MSE loss between output and ground truth pairs or maximizing the likelihood on large-scale data, they clearly outperform earlier algorithms based on natural or statistical priors [9], [11], [10], [12], [14], in terms of PSNR and SSIM. Especially, for both indoor and outdoor synthetic images, DehazeNet [15] achieves the highest PSNR value and AOD-Net [17] obtains the best SSIM score, while CAP [13] obtains the suboptimal PSNR and SSIM on indoor and outdoor images, respectively.

However, when it comes to no-reference metrics, the results become less consistent. AOD-Net [17] still maintains competitive performance by obtaining the best BLIINDS-II result on indoor images, and the best SSEQ result on outdoor images. On the other hand, several prior-based methods, such as DCP [9], FVR [10], BCCR [11] and NLD [14], also show competitiveness: FVR [10] ranks first in term of SSEQ on indoor images, and BCCR [11] wins on outdoor images in term of BLIINDS-II. We visually observe the results, and find that DCP [9], BCCR [11] and NLD [14] tend to produce sharp edges and highly contrasting colors, which explains why they are preferred by BLIINDS-II and SSEQ. Such an inconsistency between full- and no-reference evaluations aligns with the

previous argument [39] that existing objective IQA models are very limited in providing proper quality predictions of dehazed images.

B. Subjective Comparison on HSTS

We recruit 100 participants from different educational backgrounds for the subjective survey as described in Section 4.2, using HSTS which contains 10 synthetic outdoor and 10 real-world hazy images. We fit a Bradley-Terry [46] model to estimate the subjective score for each method so that they can be ranked. In the Bradley-Terry model, the probability that an object X is favored over Y is assumed to be

$$p(X \succ Y) = \frac{e^{s_X}}{e^{s_X} + e^{s_Y}} = \frac{1}{1 + e^{s_Y - s_X}}, \quad (4)$$

where s_X and s_Y are the subjective scores for X and Y . The scores s for all the objects can be jointly estimated by maximizing the log likelihood of the pairwise comparison observations:

$$\max_s \sum_{i,j} w_{ij} \log \left(\frac{1}{1 + e^{s_j - s_i}} \right), \quad (5)$$

where w_{ij} is the (i, j) -th element in the winning matrix \mathbf{W} , representing the number of times when method i is favored over method j . We use the Newton-Raphson method to solve Eq. (5). Note that for a synthetic image, we have a 10×10 winning matrix \mathbf{W} , including the ground truth and nine dehazing methods results. For a real-world image, its winning matrix \mathbf{W} is 9×9 due to the absence of ground truth. For

²We highlight the top-3 performances using red, cyan and blue, respectively.

synthetic images, we set the score for ground truth method as 1 to normalization scores.

Figures 4 and 5 show qualitative examples of dehazed results on a synthetic and a real-world image, respectively. Quantitative results can be found in Table V and the trends are visualized in Figure 3. We also compute the full- and no-reference metrics on synthetic images to examine their consistency with the subjective scores.

A few interesting observations could be drawn:

- The subjective qualities of various algorithms' results show different trends on synthetic and real hazy images. On the 10 synthetic images of HSTS, DCP [9] receives the best clearness score and DehazeNet the best in authenticity score. On the 10 real images, CNN-based methods [15], [16], [17] rank top-3 in terms of both clearness and authenticity, in which MSCNN [16] achieves the best according to both scores.
- The clearness and authenticity scores of the same image are often not aligned. As can be seen from Figure 3, the two subjective scores are hardly correlated on synthetic images; their correlation shows better on real images. That reflects the complexity and multi-facet nature of subjective perceptual evaluation.
- From Table V, we observe the divergence between subjective and objective (both full- and no-reference) evaluation results. For the best performer in subjective evaluation, MSCNN [16], its PSNR/SSIM results on synthetic indoor images are quite low, while SSEQ/BLIINDS-II on both synthetic and outdoor images are moderate. As another example, GRM [12] receives the highest SSEQ/BLIINDS-II scores on real HSTS images. However both of its subjective scores rank only fifth among nine algorithms on the same set.

C. Task-driven Comparison on RTTS

We adopt the commonly used Faster R-CNN [48]³, and use the same fixed model to detect objects from the dehazed results, over the RTTS images. Figure 6 compares the object detection results on an RTTS hazy image and after applying nine different dehazing algorithms⁴.

Table VI compares all mAP results, from which we can see that BCCR [11] and MSCNN [16] are two best performers, implying that both traditional and CNN-based methods have good potential to contribute to object detection. On the other hand, if comparing the ranking of detection mAP with the no-reference results on the same set, we can again only observe a weak correlation. For example, BCCR [11] achieves highest BLIINDS-II value, but MSCNN has lower SSEQ and BLIINDS-II scores than most competitors. That manifests the necessity of evaluating in a task-driven way.

Discussion: Optimizing Detection Performance in Haze? [17] for the first time reported the promising performance on

³Here we used `py-faster-rcnn` and its VGG16 based model trained on VOC2007 trainval dataset.

⁴For FVR, only 3,966 images are counted, since for the remaining 356 FVR fails to provide any reasonable result.

TABLE VI
DETECTION RESULTS ON RTTS.

	mAP	Person	Bicycle	Car	Bus	Motorbike
RawHaze	0.38	0.61	0.41	0.35	0.21	0.30
DCP [9]	0.41	0.62	0.41	0.42	0.24	0.34
FVR [10]	0.35	0.58	0.39	0.35	0.19	0.25
BCCR [11]	0.42	0.62	0.45	0.43	0.25	0.34
GRM [12]	0.29	0.50	0.31	0.26	0.15	0.22
CAP [13]	0.40	0.61	0.40	0.42	0.25	0.30
NLD [14]	0.40	0.61	0.40	0.42	0.24	0.33
DehazeNet [15]	0.41	0.61	0.41	0.42	0.25	0.34
MSCNN [16]	0.41	0.61	0.42	0.43	0.25	0.36
AOD-Net [17]	0.37	0.61	0.40	0.35	0.21	0.30

detecting objects in the haze, by concatenating and jointly tuning AOD-Net with Faster-RCNN as one unified pipeline, following [49], [50]. The authors trained their detection pipeline using an annotated dataset of synthetic hazy images, generated from VOC2007 [45]. Due to the absence of annotated realistic hazy images, they only reported quantitative performance on a separate set of synthetic annotated images. While their goal is different from the scope of RTTS (where a fixed Faster-RCNN is applied on dehazing results for fair comparison), we are interested to explore whether we could further boost the detection mAP on RTTS realistic hazy images using such a joint pipeline.

In order for further enhancing the performance of such a dehazing + detection joint pipeline in realistic hazy photos or videos, there are at least two other noteworthy potential options as we can see for future efforts:

- Developing *photo-realistic* simulation approaches of generating hazy images from clean ones [51], [52]. That would resolve the bottleneck of handle-labeling and supply large-scale annotated training data with little mismatch. The technique of haze severity estimation [53] may also help the synthesis, by first estimating the haze level from (unannotated) testing images and then generating training images accordingly.
- If we view the synthetic hazy images as the source domain (with abundant labels) and the realistic ones as the target domain (with scarce labels), then the unsupervised domain adaption can be performed to reduce the domain gap in low-level features, by exploiting unannotated realistic hazy images. For example, [54] provided an example of pre-training the robust low-level CNN filters using unannotated data from both source and target domains, leading to much improved robustness when applied to testing on the target domain data. For this purpose, we have included 4,322 unannotated realistic hazy images in RESIDE that might help build such models.

Apparently, the above discussions can be straightforwardly applied to other high-level vision tasks in uncontrolled outdoor environments (e.g., bad weathers and poor illumination), such as tracking, recognition, semantic segmentation, etc.

D. Running Time

Table VIII reports the per-image running time of each algorithm, averaged over the synthetic indoor images (620×460) in SOTS, using a machine with 3.6 GHz CPU and 16G RAM.

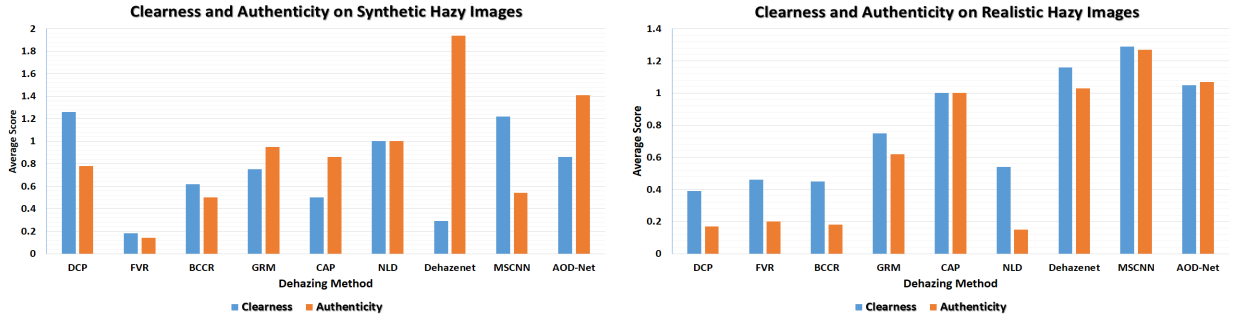


Fig. 3. Averaged clearness and authenticity scores: (a) on 10 synthetic images in HSTS; and (b) on real-world images in HSTS.

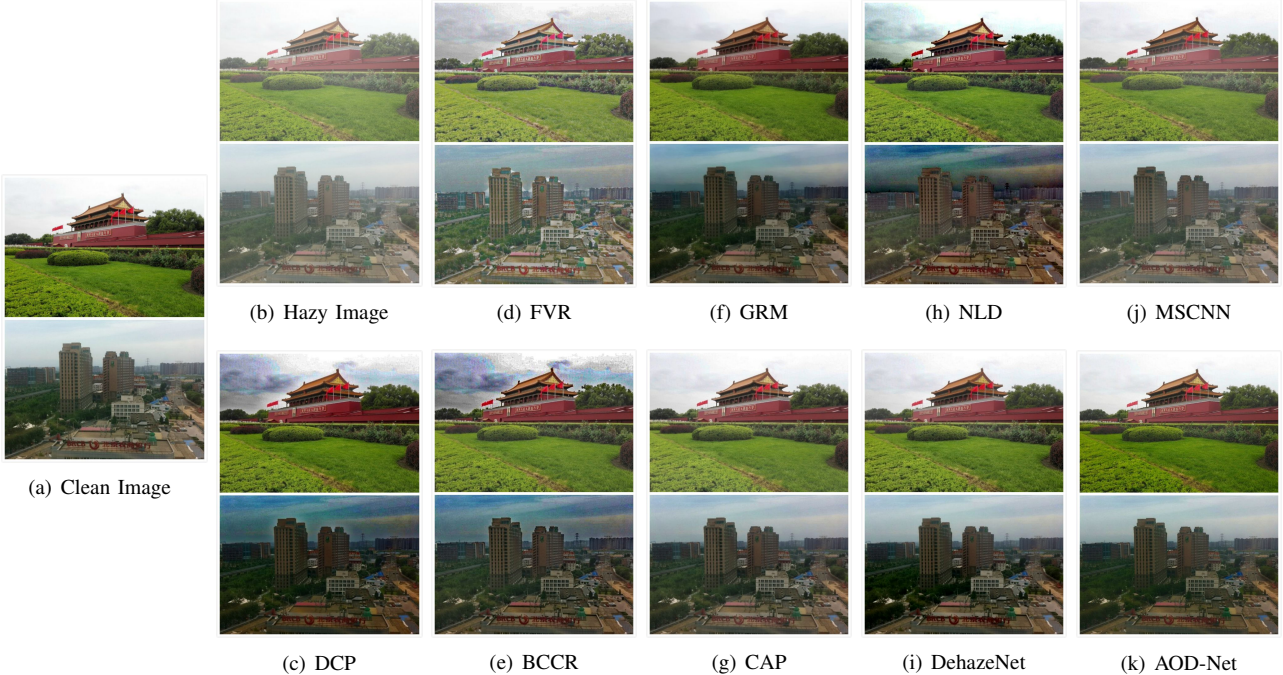


Fig. 4. Examples of dehazed results on a synthetic hazy image from HSTS.

TABLE VII
AVERAGE NO-REFERENCE METRICS OF DEHAZED RESULTS ON RTTS.

	DCP [9]	FVR [10]	BCCR [11]	GRM [12]	CAP [13]	NLD [14]	DehazeNet [15]	MSCNN [16]	AOD-Net [17]
SSEQ	62.87	63.59	63.31	58.64	60.66	59.37	60.01	62.31	65.35
BLIINDS-II	68.34	67.68	74.07	54.54	65.15	68.32	52.54	56.59	71.05

TABLE VIII
COMPARISON OF AVERAGE PER-IMAGE RUNNING TIME (SECOND) ON SYNTHETIC INDOOR IMAGES IN SOTS.

Time	DCP [9]	FVR [10]	BCCR [11]	GRM [12]	CAP [13]	NLD [14]	DehazeNet [15]	MSCNN [16]	AOD-Net [17]
Time	1.62	6.79	3.85	83.96	0.95	9.89	2.51	2.60	0.65

All methods are implemented in MATLAB, except AOD-Net by Pycaffe. However, it is fair to compare AOD-Net with other methods since MATLAB implementation has superior efficiency than Pycaffe as shown in [17]. AOD-Net shows a clear advantage over others in efficiency, thanks to its light-weight feed-forward structure.

VI. CONCLUSIONS AND FUTURE WORK

In this paper, we propose the RESIDE benchmark and systematically evaluate the state-of-the-arts in single image dehazing. From the results presented, there seems to be no single-best dehazing model for all criteria: AOD-Net and DehazeNet are favored by PSNR and SSIM; DCP, FVR and BCCR are more competitive in terms of no-reference metrics; MSCNN shows to have the most appreciated subjective quality; BCCR

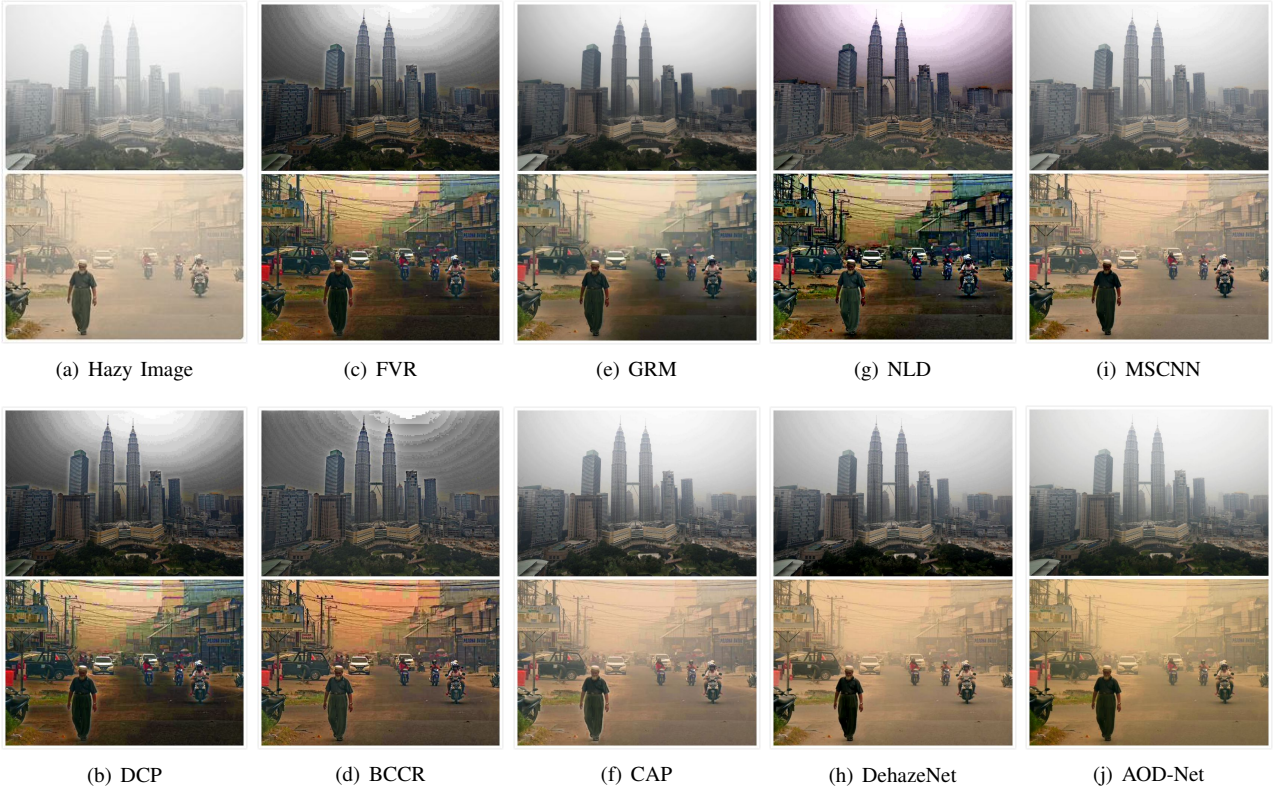


Fig. 5. Examples of dehazed results on a real-world hazy image from HSTS.

and MSCNN lead to superior detection performance on real hazy images; and finally AOD-Net is the most efficient among all. We see the highly complicated nature of the dehazing problem, in both real-world generalization and evaluation criteria. For future research, we advocate to evaluate and optimize dehazing algorithms towards more dedicated cafeterias (e.g., subjective visual quality, or high-level target task performance), rather than solely PSNR/SSIM, which are found to be poorly aligned with other metrics we used. In particular, correlating dehazing with high-level computer vision problems will likely lead to innovative robust computer vision pipelines that will find many immediate applications. Another blank to fill is developing no-reference metrics that are better correlated with human perception, for evaluating dehazing results. That progress will accelerate the needed shift from current full-reference evaluation on only synthetic images, to the more realistic evaluation schemes with no ground truth.

ACKNOWLEDGEMENT

We appreciate the support from the authors of [14], [18]. We acknowledge Dr. Changxing Ding, South China University of Technology, for his indispensable support to our data collection and cleaning.

REFERENCES

- [1] “How autonomous vehicles will navigate bad weather remains foggy,” <https://www.forbes.com/sites/centurylink/2016/11/29/how-autonomous-vehicles-will-navigate-bad-weather-remains-foggy/#1aff07088662>. 1
- [2] S. G. Narasimhan and S. K. Nayar, “Contrast restoration of weather degraded images,” *IEEE transactions on pattern analysis and machine intelligence*, vol. 25, no. 6, pp. 713–724, 2003. 1
- [3] Y. Y. Schechner, S. G. Narasimhan, and S. K. Nayar, “Instant dehazing of images using polarization,” in *Computer Vision and Pattern Recognition, 2001. CVPR 2001. Proceedings of the 2001 IEEE Computer Society Conference on*, vol. 1. IEEE, 2001, pp. I-I. 1
- [4] T. Treibitz and Y. Y. Schechner, “Polarization: Beneficial for visibility enhancement?” in *Computer Vision and Pattern Recognition, 2009. CVPR 2009. IEEE Conference on*. IEEE, 2009, pp. 525–532. 1
- [5] J. Kopf, B. Neubert, B. Chen, M. Cohen, D. Cohen-Or, O. Deussen, M. Uyttendaele, and D. Lischinski, “Deep photo: Model-based photograph enhancement and viewing,” in *ACM transactions on graphics (TOG)*, vol. 27, no. 5. ACM, 2008, p. 116. 1
- [6] E. J. McCartney, “Optics of the atmosphere: scattering by molecules and particles,” *New York, John Wiley and Sons, Inc.*, 1976. 421 p., 1976. 1
- [7] S. G. Narasimhan and S. K. Nayar, “Chromatic framework for vision in bad weather,” in *Computer Vision and Pattern Recognition, 2000. Proceedings. IEEE Conference on*, vol. 1. IEEE, 2000, pp. 598–605. 1
- [8] ——, “Vision and the atmosphere,” *International Journal of Computer Vision*, vol. 48, no. 3, pp. 233–254, 2002. 1
- [9] K. He, J. Sun, and X. Tang, “Single image haze removal using dark channel prior,” in *IEEE Conference on Computer Vision and Pattern Recognition*, 2009. 1, 5, 6, 7, 8
- [10] J.-P. Tarel and N. Hautiere, “Fast visibility restoration from a single color or gray level image,” in *IEEE International Conference on Computer Vision*, 2009. 1, 5, 6, 7, 8
- [11] G. Meng, Y. Wang, J. Duan, S. Xiang, and C. Pan, “Efficient image dehazing with boundary constraint and contextual regularization,” in *IEEE International Conference on Computer Vision*, 2013. 1, 5, 6, 7, 8
- [12] C. Chen, M. N. Do, and J. Wang, “Robust image and video dehazing with visual artifact suppression via gradient residual minimization,” in *European Conference on Computer Vision*, 2016. 1, 5, 6, 7, 8
- [13] Q. Zhu, J. Mai, and L. Shao, “A fast single image haze removal algorithm using color attenuation prior,” *IEEE Transactions on Image Processing*, vol. 24, no. 11, pp. 3522–3533, 2015. 1, 5, 6, 7, 8
- [14] D. Berman, S. Avidan *et al.*, “Non-local image dehazing,” in *IEEE*

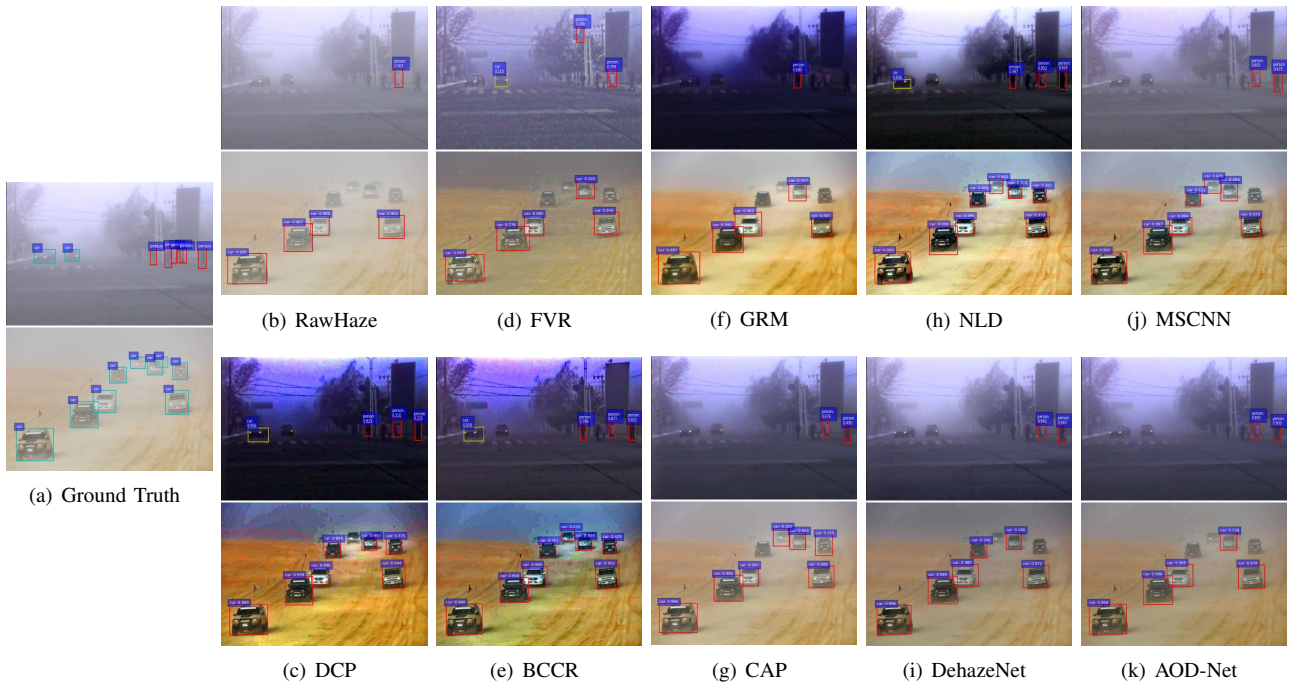


Fig. 6. Visualization of two RTTS images' object detection results after applying different dehazing algorithms.

- Conference on Computer Vision and Pattern Recognition*, 2016. 1, 2, 5, 6, 7, 8, 9
- [15] B. Cai, X. Xu, K. Jia, C. Qing, and D. Tao, "Dehazenet: An end-to-end system for single image haze removal," *IEEE Transactions on Image Processing*, vol. 25, no. 11, pp. 5187–5198, 2016. 1, 2, 4, 5, 6, 7, 8
 - [16] W. Ren, S. Liu, H. Zhang, J. Pan, X. Cao, and M.-H. Yang, "Single image dehazing via multi-scale convolutional neural networks," in *European Conference on Computer Vision*, 2016. 1, 2, 4, 5, 6, 7, 8
 - [17] B. Li, X. Peng, Z. Wang, J. Xu, and D. Feng, "Aod-net: All-in-one dehazing network," in *IEEE International Conference on Computer Vision*, 2017. 1, 2, 4, 5, 6, 7, 8
 - [18] R. Fattal, "Single image dehazing," *ACM transactions on graphics (TOG)*, vol. 27, no. 3, p. 72, 2008. 1, 9
 - [19] K. He, J. Sun, and X. Tang, "Single image haze removal using dark channel prior," *IEEE transactions on pattern analysis and machine intelligence*, vol. 33, no. 12, pp. 2341–2353, 2011. 1
 - [20] K. Tang, J. Yang, and J. Wang, "Investigating haze-relevant features in a learning framework for image dehazing," in *Proceedings of the IEEE Conference on Computer Vision and Pattern Recognition*, 2014, pp. 2995–3000. 1
 - [21] Z. Li, P. Tan, R. T. Tan, D. Zou, S. Zhiying Zhou, and L.-F. Cheong, "Simultaneous video defogging and stereo reconstruction," in *Proceedings of the IEEE Conference on Computer Vision and Pattern Recognition*, 2015, pp. 4988–4997. 2
 - [22] L. Kratz and K. Nishino, "Factorizing scene albedo and depth from a single foggy image," in *Computer Vision, 2009 IEEE 12th International Conference on*. IEEE, 2009, pp. 1701–1708. 2
 - [23] K. Nishino, L. Kratz, and S. Lombardi, "Bayesian defogging," *International journal of computer vision*, vol. 98, no. 3, pp. 263–278, 2012. 2
 - [24] D. Nair, P. A. Kumar, and P. Sankaran, "An effective surround filter for image dehazing," in *Proceedings of the 2014 International Conference on Interdisciplinary Advances in Applied Computing*. ACM, 2014, p. 20. 2
 - [25] J. Zhou and F. Zhou, "Single image dehazing motivated by retinex theory," in *Instrumentation and Measurement, Sensor Network and Automation (IMSNA), 2013 2nd International Symposium on*, 2013, pp. 243–247. 2
 - [26] B. Li, X. Peng, Z. Wang, J. Xu, and D. Feng, "End-to-end united video dehazing and detection," *arXiv preprint arXiv:1709.03919*, 2017. 2
 - [27] H. R. Sheikh, M. F. Sabir, and A. C. Bovik, "A statistical evaluation of recent full reference image quality assessment algorithms," *IEEE Transactions on image processing*, vol. 15, no. 11, pp. 3440–3451, 2006. 2
 - [28] E. Agustsson and R. Timofte, "Ntire 2017 challenge on single image super-resolution: Dataset and study," in *The IEEE Conference on Computer Vision and Pattern Recognition (CVPR) Workshops*, vol. 3, 2017. 2
 - [29] R. Fattal, "Dehazing using color-lines," *ACM Transactions on Graphics (TOG)*, vol. 34, no. 1, p. 13, 2014. 2
 - [30] C. Sakaridis, D. Dai, and L. Van Gool, "Semantic foggy scene understanding with synthetic data," *arXiv preprint arXiv:1708.07819*, 2017. 2, 3, 4, 5
 - [31] F. Liu, C. Shen, G. Lin, and I. Reid, "Learning depth from single monocular images using deep convolutional neural fields," *IEEE transactions on pattern analysis and machine intelligence*, vol. 38, no. 10, pp. 2024–2039, 2016. 2, 4
 - [32] J.-P. Tarel, N. Hautiere, L. Caraffa, A. Cord, H. Halimaoui, and D. Gruyer, "Vision enhancement in homogeneous and heterogeneous fog," *IEEE Intelligent Transportation Systems Magazine*, vol. 4, no. 2, pp. 6–20, 2012. 2
 - [33] N. Silberman, D. Hoiem, P. Kohli, and R. Fergus, "Indoor segmentation and support inference from rgbd images," in *European Conference on Computer Vision*. Springer, 2012, pp. 746–760. 3, 4, 5
 - [34] D. Scharstein and R. Szeliski, "High-accuracy stereo depth maps using structured light," in *Computer Vision and Pattern Recognition, 2003. Proceedings. 2003 IEEE Computer Society Conference on*, vol. 1. IEEE, 2003, pp. I–I. 3, 4
 - [35] A. Saxena, M. Sun, and A. Y. Ng, "Make3d: Learning 3d scene structure from a single still image," *IEEE transactions on pattern analysis and machine intelligence*, vol. 31, no. 5, pp. 824–840, 2009. 3, 4
 - [36] A. Mittal, A. K. Moorthy, and A. C. Bovik, "No-reference image quality assessment in the spatial domain," *IEEE Transactions on Image Processing*, vol. 21, no. 12, pp. 4695–4708, 2012. 4
 - [37] M. A. Saad, A. C. Bovik, and C. Charrier, "Blind image quality assessment: A natural scene statistics approach in the dct domain," *IEEE transactions on Image Processing*, vol. 21, no. 8, pp. 3339–3352, 2012. 4, 5
 - [38] L. Liu, B. Liu, H. Huang, and A. C. Bovik, "No-reference image quality assessment based on spatial and spectral entropies," *Signal Processing: Image Communication*, vol. 29, no. 8, pp. 856–863, 2014. 4, 5
 - [39] K. Ma, W. Liu, and Z. Wang, "Perceptual evaluation of single image dehazing algorithms," in *Image Processing (ICIP), 2015 IEEE International Conference on*. IEEE, 2015, pp. 3600–3604. 4, 5, 6
 - [40] Z. Chen, T. Jiang, and Y. Tian, "Quality assessment for comparing image enhancement algorithms," in *Proceedings of the IEEE Conference on Computer Vision and Pattern Recognition*, 2014, pp. 3003–3010. 4
 - [41] "Beijing realtime weather photos," <http://goo.gl/svzxLm>. 4

- [42] A. Geiger, P. Lenz, and R. Urtasun, "Are we ready for autonomous driving? the kitti vision benchmark suite," in *Computer Vision and Pattern Recognition (CVPR), 2012 IEEE Conference on*. IEEE, 2012, pp. 3354–3361. [4](#)
- [43] F. Ma and S. Karaman, "Sparse-to-dense: Depth prediction from sparse depth samples and a single image," *arXiv preprint arXiv:1709.07492*, 2017. [4](#)
- [44] L. Wang, H. Jin, R. Yang, and M. Gong, "Stereoscopic inpainting: Joint color and depth completion from stereo images," in *Computer Vision and Pattern Recognition, 2008. CVPR 2008. IEEE Conference on*. IEEE, 2008, pp. 1–8. [4](#)
- [45] M. Everingham, L. Van Gool, C. K. I. Williams, J. Winn, and A. Zisserman, "The PASCAL Visual Object Classes Challenge 2007 (VOC2007) Results," <http://www.pascal-network.org/challenges/VOC/voc2007/workshop/index.html>. [5](#), [7](#)
- [46] R. A. Bradley and M. E. Terry, "Rank analysis of incomplete block designs: I. the method of paired comparisons," *Biometrika*, vol. 39, no. 3/4, pp. 324–345, 1952. [5](#), [6](#)
- [47] D. Liu, D. Wang, and H. Li, "Recognizable or not: Towards image semantic quality assessment for compression," *Sensing and Imaging*, vol. 18, no. 1, p. 1, 2017. [5](#)
- [48] S. Ren, K. He, R. Girshick, and J. Sun, "Faster r-cnn: Towards real-time object detection with region proposal networks," in *Advances in Neural Information Processing Systems*. [5](#), [7](#)
- [49] Z. Wang, S. Chang, Y. Yang, D. Liu, and T. S. Huang, "Studying very low resolution recognition using deep networks," in *Proceedings of the IEEE Conference on Computer Vision and Pattern Recognition*, 2016, pp. 4792–4800. [7](#)
- [50] B. Cheng, Z. Wang, Z. Zhang, Z. Li, J. Yang, and T. S. Huang, "Robust emotion recognition from low quality and low bit rate video: A deep learning approach," in *Proceedings of the 7-th Conference on Affective Computing and Intelligent Interaction*, 2017. [7](#)
- [51] A. Shrivastava, T. Pfister, O. Tuzel, J. Susskind, W. Wang, and R. Webb, "Learning from simulated and unsupervised images through adversarial training," *arXiv preprint arXiv:1612.07828*, 2016. [7](#)
- [52] K. Li, Y. Li, S. You, and N. Barnes, "Photo-realistic simulation of road scene for data-driven methods in bad weather," in *Proceedings of the IEEE Conference on Computer Vision and Pattern Recognition Worksho*, 2017, pp. 491–500. [7](#)
- [53] Y. Li, J. Huang, and J. Luo, "Using user generated online photos to estimate and monitor air pollution in major cities," in *Proceedings of the 7th International Conference on Internet Multimedia Computing and Service*. ACM, 2015, p. 79. [7](#)
- [54] Z. Wang, J. Yang, H. Jin, E. Shechtman, A. Agarwala, J. Brandt, and T. S. Huang, "Deepfont: Identify your font from an image," in *Proceedings of the 23rd ACM international conference on Multimedia*. ACM, 2015, pp. 451–459. [7](#)